Monthly Notices
of the
ROYAL ASTRONOMICAL SOCIETY
MNRAS (2017) doi:10.1093/mnras/stx672

Optical thickness, spin temperature and correction factor for the density of Galactic H I gas

Yoshiaki Sofue★
Insitute of Astronomy, University of Tokyo, Mitaka, Tokyo 181-0015, Japan

Accepted 2017 March 15. Received 2017 March 10; in original form 2016 December 24

ABSTRACT

This paper presents a method to determine the spin temperature of the local ($V_{\rm LSR}$ = 0 km s^{-1}) H I gas using the saturated brightness temperature of the 21-cm line in radial velocity-degenerate regions (VDRs). The spin temperature is determined to be: $T_{\rm S} = 146.2 \pm 16.1$ K by measuring saturated brightness in the VDR towards the Galactic Centre; 146.8 ± 10.7 K by χ^2 fitting of the expected brightness distribution to observations around the VDR; and 144.4 ± 6.8 K towards the local arm. Assuming $T_{\rm S} = 146$ K, a correction factor Γ for the H I density, defined by the ratio of the true H I density for finite optical thickness to that calculated by assuming optically thin H I, was obtained as $\Gamma \sim 1.2$ (optical depth $\tau \sim 0.3$) in the local H I gas, ∼1.8 (∼1.3) towards the arm and anti-Centre, and as high as ∼3.6 (∼2.7) in the Galactic Centre direction. It is suggested that the H I density and mass in the local arm could be ∼2 times greater than currently estimated values, and that in the inner Galaxy could be ∼3.6 times greater.

Key words: ISM: atoms – ISM: general – local interstellar matter – galaxies: ISM.

1 INTRODUCTION

The density of Galactic H I gas is usually calculated approximately using the two assumptions that the 21-cm line is optically thin and that the background continuum emission is sufficiently weak. This approximation is convenient, because the spin temperature of H I does not appear in the conversion relation from observed H I intensity to the hydrogen volume or column density. However, the approximation significantly underestimates the H I density, when the two assumptions are not valid. Precise densities can be estimated using a general conversion relation including both the spin temperature and continuum brightness for finite optical thickness of the H I line.

The H I line emission is often observed to have brightness temperatures as high as $T_{\rm B} \sim$ several tens to ∼100 K (e.g. Kalberla et al. 2005), comparable to the spin temperature, $T_{\rm S}$, indicating that the optical thickness may not be so small. Also, radio continuum emission of the Galactic disc is not sufficiently weak in the inner Galaxy that it can be ignored. In such regions, the continuum emission is absorbed by the H I gas, causing apparently lower H I brightness, and leading to lower H I density by the thin assumption than the true value.

Thus, the optically thin assumption may not be valid in regions having high H I brightness and/or bright continuum background. Moreover, such regions are predominantly distributed in the Galactic plane, so that the H I density and mass in the Galactic disc may have been significantly underestimated.

The spin (excitation) temperature, $T_{\rm S}$, of the interstellar H I gas has been studied extensively by analysing the emission and absorption profiles of 21-cm line spectra towards individual H I clouds, molecular clouds and/or dark clouds located in front of Galactic and extragalactic radio continuum sources (Mebold et al. 1982; Liszt 1983, 2001; Kuchar & Bania 1990; Liszt, Braun & Greisen 1993; Roberts et al. 1993; Stark et al. 1994; Wolfire et al. 1995; Dickey et al. 2003; Heiles & Troland 2003a,b; Li & Goldsmith 2003; Goldsmith & Li 2005; Chengalur, Kanekar & Roy 2013; Roy et al. 2013a; Roy, Kanekar & Chengalur 2013b; Brown et al. 2014; Fukui et al. 2014, 2015; Lee et al. 2015; Murray et al. 2015). The currently measured temperatures range from $T_{\rm S} \sim 20$ to ∼300 K for the cold H I component, and from $T_{\rm S} \sim 2000$ to ∼10 000 K for the warm component, corresponding to the cold (CNM) and warm (WNM) neutral material of the two stable phases of the interstellar pressure equilibrium (Field, Goldsmith & Habing 1969). In these studies, analyses have been made by using 21-cm line profiles in the velocity (frequency) space, and the observations have been obtained along specific lines of sight in the directions of radio continuum sources.

In the present paper, we propose a method to measure the mean spin temperature of H I gas in the Galactic disc, and we apply it to the H I brightness distribution in the directions of velocity-degenerate regions (VDRs) towards the Galactic Centre (GC), anti-Centre and tangential directions to the solar circle. In these directions, especially towards the GC, the H I line intensity at $V_{\rm LSR} \sim 0$ km s^{-1} is almost saturated because of the large optical depth

★ E-mail: sofue@ioa.s.u-tokyo.ac.jp

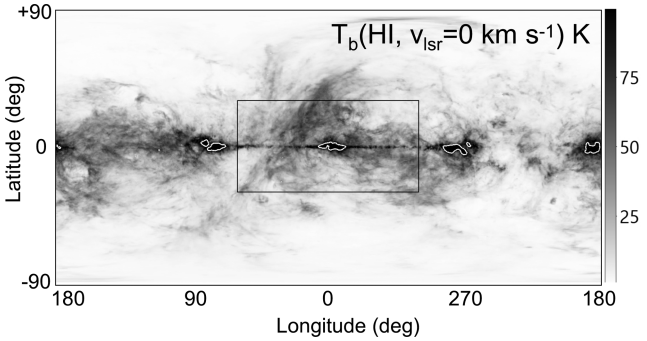

Figure 1. H I T_B distribution on the sky at $V_{LSR} = 0$ km s^{-1} from the LAB H I survey (Kalberla et al. 2005). White contours are at $T_B = 100$ K, approximately enclosing the radial VDRs. The square shows the analysed region in this study.

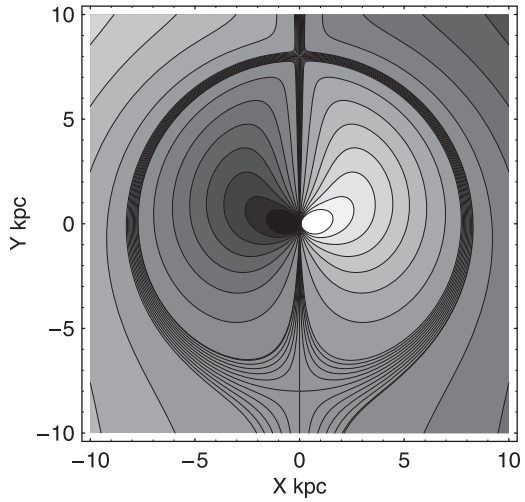

Figure 2. VDR at $-5 \le V_{LSR} \le +5$ km s^{-1} indicated by dense contours with 1 km s^{-1} intervals in the radial velocity field of the Galaxy, calculated for the rotation curve of the potential of Miyamoto & Nagai (1975). Other contours are at every ± 20 km s^{-1}. The Sun is at $X = 0$, $Y = R_0 = 8$ kpc, and the rotation velocity is $V_0 = 200$ km s^{-1}.

Using the measured spin temperature T_S, we derive the optical depth τ of the H I line, and we obtain a correction factor Γ to convert the H I density calculated under the optically thin assumption to a more general and reliable density for finite optical thickness. In the analyses, we make use of the Leiden–Argentine–Bonn (LAB) all-sky H I survey (Kalberla et al. 2005) and the Rhodes 2300-MHz radio continuum survey (Jonas, de Jager & Baart 1985).

2 DATA

2.1 H I map

Fig. 1 shows the distribution of the H I line brightness temperature, T_B, at $V_{LSR} = 0$ km s^{-1} as taken from the LAB H I survey at a spatial resolution of 0.°6 FWHM (Kalberla et al. 2005). Because the channel velocity interval is 1.0 km s^{-1} and the velocity resolution of the survey is 1.3 km s^{-1}, the emission comes approximately from the shaded region shown in Fig. 2, considering the velocity dispersion of $\sim$10 ($\pm$5) km s^{-1}. Most off-Galactic plane emission comes from local H I gas near the Sun, whereas emission from the VDR (e.g. regions in the Galactic plane towards the GC, anti-Centre

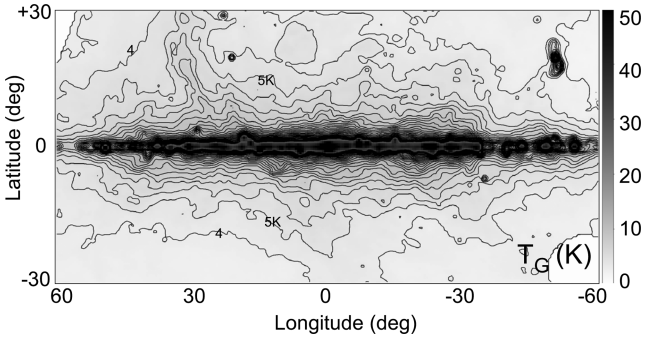

Figure 3. Galactic 1.4-GHz radio continuum map of T_G, as converted from the 2.3-GHz Rhodes map (Jonas et al. 1985) for an assumed spectral index $\beta = -2.7$. Contour interval is 1 K. A map of $T_C = T_G + T_{CMB}$ is used for analysis of local H I.

and tangential directions of the solar circle) comes through the long path in the Galactic disc (Fig. 2). In Fig. 1, we show the VDRs as regions approximately enclosed by contours at $T_B = 100$ K. We use the saturated H I brightness in the VDRs to determine the spin temperature.

To determine the local H I gas density around the Sun, we analyse the rectangular region indicated in Fig. 1, and we use off-Galactic plane data at $|b| > 1^\circ$ in order to avoid the contamination of far-side H I emission along the solar circle.

The map partially includes the outskirts line emission from the Aquila Rift, which is located $\sim$200 pc away from the Sun corresponding to the centre velocity of $V_{LSR} \sim 4$ km s^{-1}, having a linewidth of several km s^{-1} (Sofue & Nakanishi 2017a). In order to reduce such contamination from individual objects, we average the values in regions as wide as possible in the box shown in Fig. 1.

2.2 Radio continuum map

Fig. 3 shows the brightness distribution of radio continuum emission T_C at 1420 MHz, as converted from the Rhodes 2300-MHz survey (Jonas et al. 1985). The brightness temperature at 2300 MHz was converted to that at 1420 MHz for an assumed spectral index of $\beta_{synch} = -2.7$ as

$$T_C = T_C(\nu_1)(\nu_2/\nu_1)^{\beta_{synch}} + T_{CMB}, \quad (1)$$

where $\nu_1 = 2300$ MHz and $\nu_2 = 1420$ MHz. The assumption of synchrotron emission in the off-Galactic plane region is plausible, because thermal sources such as H II regions are highly concentrated towards the Galactic plane in a thin disc with a full thickness of $\sim$90 pc, or $|b| < \sim 0.^\circ 3$.

However, for the analysis of emission in the Galactic plane, we assume that the Galactic continuum emission is an equal mixture of thermal and non-thermal emissions, as given by

$$T_C = T_C(\nu_1)\left[\eta\left(\frac{\nu_2}{\nu_1}\right)^{\beta_{synch}} + (1-\eta)\left(\frac{\nu_2}{\nu_1}\right)^{\beta_{therm}}\right] + T_{CMB}, \quad (2)$$

where the spectral indices for synchrotron and thermal radiations are assumed to be $\beta_{synch} = -2.7$ and $\beta_{therm} = -2$, respectively. Here, η is the fractional ratio of the non-thermal and thermal emissions at ν_1. Separation of the non-thermal and thermal contributions of the radio continuum emission in the Galactic plane has shown that the ratio of the non-thermal to thermal brightness temperatures at 600 MHz is $\sim$2.5 at $|l| < \sim 30^\circ$ (Large, Mathewson & Haslam 1961). This ratio corresponds to $\eta \sim 0.5$ at $\nu_1 = 2.3$ GHz for the above spectral indices. So, here we adopt this value in equation (2).

The 2300-MHz map was used to avoid the absorption effect by H I in the 1420-MHz map. We confirm that the converted intensities at 1420 MHz are consistent with that directly observed at the 1420-MHz continuum at $l = 15^\circ$–30° (Sofue & Reich 1979).

3 METHOD

3.1 H I emission and absorption

The observed brightness temperature $T_{\rm B}$ of the H I line emission from an H I emitting source with spin (excitation) temperature $T_{\rm S}$ is given by

$$T_{\rm B} = (T_{\rm S} - T_{\rm C})(1 - {\rm e}^{-\tau}), \tag{3}$$

where τ and $T_{\rm C}$ are the optical depth and brightness temperature of background continuum emission. Therefore, the optical depth is a function of the spin, brightness and continuum temperatures as

$$\tau = -\ln\left(1 - \frac{T_{\rm B}}{T_{\rm S} - T_{\rm C}}\right). \tag{4}$$

When the H I emission source is in front of the continuum source, $T_{\rm C}$ is written as

$$T_{\rm C} = T_{\rm G} + T_{\rm CMB}, \tag{5}$$

where $T_{\rm G}$ is the Galactic background brightness and $T_{\rm CMB} = 2.7$ K is the cosmic microwave background. This equation applies even when the continuum and H I emissions originate from the same region, in so far as the region is optically thick against H I. However, if the H I source is optically thin in this case, $T_{\rm G}$ may be reduced by a factor of ∼4, because the practical H I absorption takes place against the farther-side half of the continuum source by the nearer-side half of the H I source.

For the optically thin case, the H I brightness is approximated by

$$T_{\rm B} \simeq (T_{\rm S} - T_{\rm C})\tau. \tag{6}$$

Furthermore, if the continuum background can be neglected, or $T_{\rm S} \gg T_{\rm C}$, this relation reduces to the often quoted relation:

$$\tau \simeq T_{\rm B}/T_{\rm S}. \tag{7}$$

However, for the optically thick case, $\tau \gg 1$, we have

$$T_{\rm B} \simeq T_{\rm S} - T_{\rm C}. \tag{8}$$

This relation will be used to measure $T_{\rm S}$ towards velocity-degenerate directions, where the optical depth is sufficiently large. This approximation is valid even if the continuum and H I sources are located in the same region, because the continuum emission from regions with $\tau > 1$ is regarded to be the background.

3.2 Correction factor Γ for H I density

The column density of H atoms, N, on the line of sight is calculated by

$$N = -X_{\rm H\,I} T_{\rm S} \int \ln\left(1 - \frac{T_{\rm B}}{T_{\rm S} - T_{\rm C}}\right) {\rm d}v, \tag{9}$$

where $X_{\rm H\,I} = 1.82 \times 10^{18}$ cm^{-2} (K km s^{-1})$^{-1}$ is the conversion factor. The volume density n is related to $T_{\rm B}$ as

$$n = \frac{{\rm d}N}{{\rm d}x} = -X_{\rm H\,I} T_{\rm S} \ln\left(1 - \frac{T_{\rm B}}{T_{\rm S} - T_{\rm C}}\right) \frac{{\rm d}v}{{\rm d}x}. \tag{10}$$

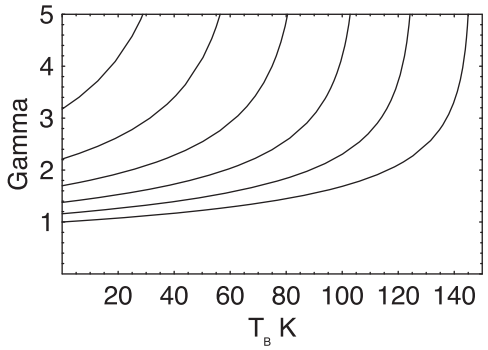

Figure 4. Correction factor Γ (ratio of volume H I density calculated for finite optical thickness to that for optically thin assumption) plotted against $T_{\rm B}$ for background continuum temperatures $T_{\rm C} = 0$ (right bottom line), 20, 40, . . . , 100 K (top left) for spin temperature of $T_{\rm S} = 146$ K.

If the H I source is optically thin, and the continuum background is weak enough (e.g. if $\tau \ll 1$ or $T_{\rm B} \ll T_{\rm S}$ and $T_{\rm C} \ll T_{\rm S}$), then these equations reduce to the often used formulae:

$$N_{\rm thin} \simeq X_{\rm H\,I} I_{\rm H\,I} = X_{\rm H\,I} \int T_{\rm B}\, {\rm d}v \tag{11}$$

and

$$n_{\rm thin} \simeq X_{\rm H\,I} T_{\rm B} \frac{{\rm d}v}{{\rm d}x}. \tag{12}$$

We introduce a correction factor Γ defined by the ratio of H I densities calculated using equations 10 and 12:

$$\Gamma = \frac{n}{n_{\rm thin}} = \frac{T_{\rm S}}{T_{\rm B}}\tau = -\frac{T_{\rm S}}{T_{\rm B}} \ln\left(1 - \frac{T_{\rm B}}{T_{\rm S} - T_{\rm C}}\right). \tag{13}$$

When $T_{\rm B} \ll T_{\rm S}$ and $T_{\rm C} \ll T_{\rm B}$, these equations reduce to $\Gamma \simeq 1$ and $\tau \simeq T_{\rm B}/T_{\rm S}$.

The correction factor Γ can be used to obtain a more general and reliable H I density, when the H I line brightness temperature is not low enough compared to the spin temperature, and/or the background continuum brightness is not negligible. Fig. 4 shows the correction factor as a function of $T_{\rm B}$ calculated for several continuum brightness temperatures.

3.3 Local H I density

Using the H I conversion factor $X_{\rm H\,I}$, we can express the volume density as

$$n = 5.89 \times 10^{-4} T_{\rm B} \frac{{\rm d}v}{{\rm d}x} \Gamma, \tag{14}$$

where $T_{\rm B}$ is measured in K and ${\rm d}v/{\rm d}x$ in km s^{-1} kpc^{-1}. When the gas is located in the solar vicinity, the velocity gradient is approximated by

$$\frac{{\rm d}v}{{\rm d}x} \simeq A\,|\sin 2l| \cos^2 b + \frac{{\rm d}\sigma}{{\rm d}x}. \tag{15}$$

Here, the first term represents the galactic rotation, $A = 14.5$ km s^{-1} kpc^{-1} is the Oort A constant and the line-of-sight derivative is related to the derivative in the Galactic plane as ${\rm d}x = {\rm d}r/\cos b$. The second term represents the velocity gradient due to turbulent motion, and is approximated by

$$\frac{{\rm d}\sigma}{{\rm d}x} \simeq \sigma/\lambda, \tag{16}$$

where λ is the line-of-sight depth.

Using the LAB H I line cube, we measured the FWHM of the H I line profile at several positions in the analysed region at $|b| > \sim 5^\circ$ to be $\sigma \sim 6$ km s^{-1}. The line-of-sight depth towards a typical inter-VDR direction at $l \sim 45^\circ$ would be $\lambda \sim \sigma/2A \sin 2l \sim 200$ pc corresponding to half σ falling to the channel at $V_{\rm LSR} = 0$ km s^{-1}. Thus, we have $\sigma/\lambda \simeq 33$ km s^{-1} kpc^{-1}, and the volume density can be estimated by

$$n \simeq 5.89 \times 10^{-4} T_{\rm B} (14.5 |\sin\ 2l| \cos^2 b + 33) \Gamma, \qquad (17)$$

with n measured in cm^{-3} and $T_{\rm B}$ in K.

4 SPIN TEMPERATURE

4.1 Methods to determine $T_{\rm S}$

In order to calculate the correction factor Γ, we need to know the spin temperature $T_{\rm S}$. There have been a number of measurements of $T_{\rm S}$ in the interstellar medium (ISM) using the emission and absorption spectra of the H I line against radio continuum sources. The measured temperatures for cold neutral ISM range from 20 to 300 K, and those for warm neutral hydrogen from ~2000 to 10^4 K (see the literature cited in Section 1).

The spin temperature of H I gas at a given frequency (velocity) can be measured by several methods. The simplest method is to compare the H I brightness temperature towards a cloud, $T_{\rm B} = (T_{\rm S} - T_{\rm C})(1 - {\rm e}^{-\tau})$, with that towards an extragalactic or Galactic continuum source located close enough inside the H I cloud, $T_{\rm B,on} = (T_{\rm S} - T_{\rm C} - T_{\rm C,on})(1 - {\rm e}^{-\tau})$ (Kuchar & Bania 1990; Liszt et al. 1993; Heiles & Troland 2003a,b; Brown et al. 2014; Murray et al. 2015). Here, $T_{\rm C,on}$ represents the continuum brightness temperature towards the absorbing continuum source, which is measured at a nearby off-line frequency. The continuum temperature $T_{\rm C,on}$ can be replaced by an absorbed brightness temperature $T_{\rm abs,on}$, by a foreground dense cloud as measured from the spectral self-absorption feature, where the H I density of the cloud has been estimated from molecular line observations (Li & Goldsmith 2003; Goldsmith & Li 2005).

Using these two relations with observed $T_{\rm B}$ and $T_{\rm B,on}$, we can eliminate the term including τ, and we can obtain the spin temperature. This method has the advantage that the measurement is accurate, if the continuum source is bright enough. However, its usage is limited only to H I clouds, where a radio continuum source is present close enough to the line of sight along which the measurement of $T_{\rm S}$ is made.

An alternative method, which we propose in this paper, is the VDR method using the saturated brightness temperature of the H I line in optically thick H I regions. For a sufficiently large optical depth, $\tau \gg 1$ – see equation (8) – the spin temperature $T_{\rm S}$ is related to the observed H I brightness temperature $T_{\rm B}$ and background continuum brightness $T_{\rm C}$ as

$$T_{\rm S} \simeq T_{\rm B} + T_{\rm C}. \qquad (18)$$

This simple method has the advantage that it can be applied to widely distributed H I gas in the Galactic disc. However, it is restricted to regions with radial velocity ranges in the VDR, where the optical depth is sufficiently large.

In the following, we apply this method to the VDR along the solar circle and the GC–Sun–anti-Centre line using the LAB H I brightness distribution at $V_{\rm LSR} = 0$ km s^{-1}, as shown in Fig. 2. Another advantage of this method is that we need no individual spectra, but we use only the brightness temperature $T_{\rm B}$ at a single frequency corresponding to the degenerate $V_{\rm LSR}$.

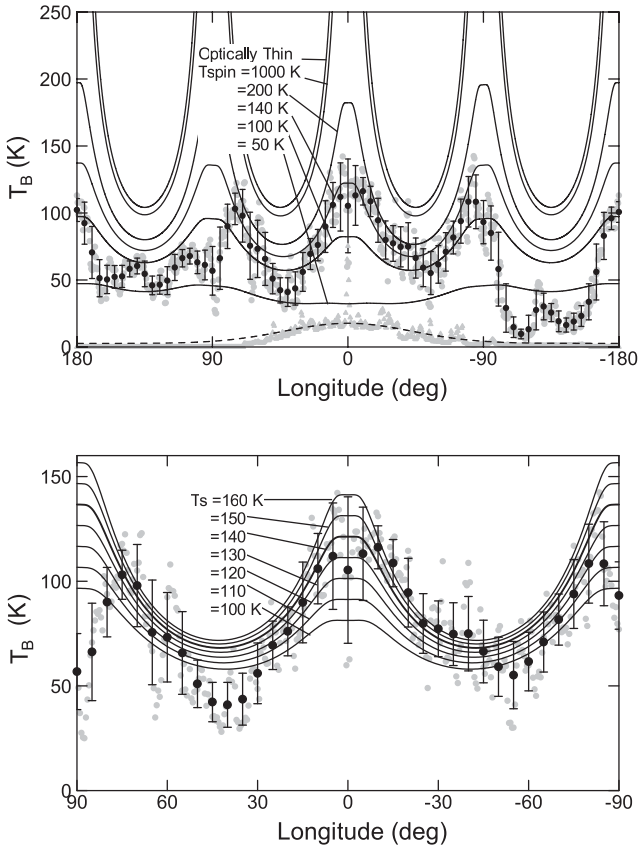

Figure 5. The top panel shows $T_{\rm B}$ along the Galactic plane at $V_{\rm LSR} = 0$ km s^{-1} for fixed H I density $n = 0.8$ H cm^{-3} and velocity range $\Delta v = 5$ km s^{-1} calculated for different $T_{\rm S}$ from 60 to 1000 K (smooth curves). Black circles show Gaussian-smoothed observed $T_{\rm B}$ at 5° longitude intervals. Bars are standard deviations. Grey dots show raw $T_{\rm B}$ before smoothing. Continuum brightness $T_{\rm C}$ is shown by grey triangles, which was approximated by the thin dashed curve in the calculation. The bottom panel is the same as the top panel but enlarged for observed and model $T_{\rm B}$ calculated for $T_{\rm S} = 100$ to 160 K every 10 K. The model curve for $T_{\rm S} = 130$ K (thick curve) fits the observations in the VDR well.

4.2 Saturated $T_{\rm B}$ in the VDR

Considering the velocity dispersion, the local H I emission at $V_{\rm LSR} \sim 0$ km s^{-1} comes from the narrow region enclosed by equal-$V_{\rm LSR}$ contours at a few km s^{-1}. The line-of-sight depth becomes large towards the four directions at $l \sim 0^\circ, \pm 90^\circ$ and ~180°, which we call the VDR (see Fig. 2).

We now consider the VDR in the directions of the GC (GC VDR) and parallel directions to the solar circle (SC VDR). In such regions, the column density at $V_{\rm LSR} = 0$ km s^{-1} is so high that the optical depth is large for CNM with the brightness temperature being nearly saturated at $T_{\rm B} \sim T_{\rm S} + T_{\rm C}$. The WNM is almost optically thin, because the absorption coefficient is inversely proportional to the spin temperature, which is as high as several thousand K.

In Fig. 1, we show the distribution of H I brightness temperature $T_{\rm B}$ at $V_{\rm LSR} = 0$ km s^{-1} on the sky from the LAB H I survey. The white contours are drawn at $T_{\rm B} = 100$ K, which approximately enclose the four VDRs. Fig. 5 shows the $T_{\rm B}$ distribution along the Galactic plane, exhibiting saturated brightness in the VDR.

The line-of-sight depths in the VDR are of the order of ~5 kpc in the solar circle, and 20 kpc in the GC. The column density along such depths for currently known H I density of $n \sim 1$ H cm^{-3} is

Table 1. Spin temperature T_S measured in the VDR.

Method/direction	T_S (K)	n (H cm^{-3})
Saturated $T_B + T_C$ in VDR[a]		
GC ($10^\circ \times 1^\circ$)	146.2 ± 16.1	–
Local arm,[b] $l = 277^\circ$ ($3^\circ \times 1^\circ$)	144.4 ± 6.8	–
χ^2 fitting in the Galactic plane, $-30^\circ \le l \le +30^\circ$	146.8 ± 10.7	0.89 ± 0.14

[a] Average in narrow boxes of ($\Delta l \times \Delta b$).
[b] Rhodes continuum data not available in the Cygnus arm.

estimated to be of the order of $N \sim$ (2–5) $\times 10^{22}$ H cm^{-2}. If the H I is CNM, the optical depth along such a long line of sight and column is much greater than unity, and the measured maximum T_B can be regarded to represent the spin temperature.

However, if the gas is WNM, the brightness temperature must be as high as $T_B \sim 10^3$ K for such a large column density, which is not the case in the four VDRs, even in the GC VDR. Thus, we can conclude that the assumption of CNM is plausible for the H I gas at $V_{LSR} \sim 0$ km s^{-1}, and the saturated values of $T_B + T_C$ in the VDR can be regarded to represent the spin temperature.

We then measured the saturated values of $T_B + T_C$ in the VDR in elliptical regions in the GC and local arm directions with l and b widths as listed in Table 1. The regions approximately trace the peak contours in Fig. 1. Thereby, we assume that T_G is a mixture of thermal and non-thermal emissions as given by equation (2).

By assuming that the saturated brightness represents the spin temperature, we thus obtain $T_S = 146.2 \pm 16.1$ K and 144.4 ± 6.8 K in the VDRs towards the GC and local arm directions, respectively. The measured values are found to be nearly constant around 145 K.

4.3 Model T_B distribution

Given the spin temperature and hydrogen density n, the H I brightness temperature at $V_{LSR} = 0$ km s^{-1} along the Galactic plane is expressed by

$$T_B = (T_S - T_C)(1 - e^{-n\, r_v / X_{H\,I} \Delta v\, T_S}). \quad (19)$$

Here, r_v is the line-of-sight depth of the region enclosed by equal-velocity contours in the velocity field, and is given by

$$r_v = |\Delta v / (A \sin 2l)|. \quad (20)$$

Thus, we have

$$T_B = (T_S - T_C) \left[1 - \exp\left(-\frac{n}{A} \sin 2l\, X_{H\,I} T_S\right)\right]. \quad (21)$$

This equation gives a good approximation in the GC direction, but it overestimates the brightness at $l \sim \pm 90^\circ$, where the line-of-sight depths are finite and the deepest lines of sight point to $l \sim \pm 80^\circ$.

The continuum contribution in the Galactic plane can be expressed as

$$T_C \simeq 16 e^{-(l/50^\circ)^2} + 2.7\,(\mathrm{K}), \quad (22)$$

approximately fitting to the observed T_C in the case of a mixture of thermal and non-thermal emission.

We now calculate the model T_B distribution as a function of longitude for an assumed density of $n = 0.8$ H cm^{-3}. In Fig. 5, we show the calculated model curves for several T_S from 50 to 1000 K, and for the optically thin case. In the lower panel, we enlarge the plots for the VDR for $T_S = 100$ to 160 K every 10 K. The model curve for $T_S =$ 140–150 K well reproduces the general characteristics of the observed T_B distribution.

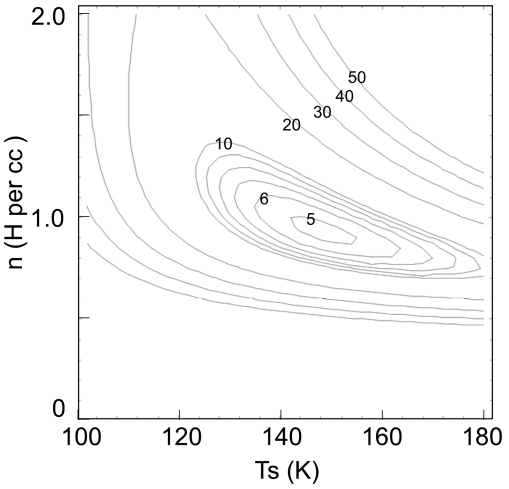

Figure 6. Contour diagram of χ^2 in the (T_S, n) plane. The best-fitting set of parameters yields $T_S = 146.8 \pm 10.7$ and $n = 0.89 \pm 0.14$ at the χ^2 minimum (= 4.75). The errors are the deviations of the parameters from the best-fitting values that increase χ^2 by 1.

According to the approximation by equation (20), the model T_B profile is identical in the four directions at $l = 0^\circ, 90^\circ, 180^\circ$ and 270°, except for the slight decrease in the GC direction due to stronger continuum emission. This approximation overestimates the line-of-sight depth in the solar circle directions, and the observed peaks at $l \pm 75^\circ$ are much lower than the model values. In the anti-Centre VDR ($l \sim 180^\circ$), the observed T_B is also lower, which is because of the lower density in the outer Galaxy.

Model curves for higher spin temperature than $\geq\sim$150 K, including high temperatures corresponding to WNM, cannot reproduce the observation. Also, curves for lower temperatures than $\leq\sim$120 K cannot fit the observation. Thus, we can confirm that the estimated local spin temperature of $T_S \sim 145$ K is reasonable.

4.4 χ^2 fit to T_B distribution

We now try to determine the spin temperature in a more statistical way by fitting the T_B distribution by the least χ^2 method. Thereby, the spin temperature T_S and the H I volume density n are taken as the two free parameters. Using equation (21), we calculate χ^2 by

$$\chi^2 = \Sigma_i (T_{B,i} - T_{B,\,\mathrm{calc}})^2 / \sigma_i^2. \quad (23)$$

Here, $T_{B,\,i}$ and σ_i are the measured brightness temperature and its standard deviation as plotted in Fig. 5 by black dots and error bars, and $T_{B,\,\mathrm{calc}}$ is the calculated temperature using equation (21), which includes T_S and n as the two free parameters. Thus, we apply the χ^2 fitting to data at $-30^\circ \le l \le +30^\circ$, where equation (20) gives a good approximation. Here, we used observed T_C instead of the model by equation (22).

In Fig. 6, we show the calculated variation of χ^2 in the T_S–n space. The best-fitting pair of T_S and n was determined so that it made the least χ^2 minimum. The errors are the deviations from the best-fitting values that increase χ^2 by 1 from its minimum.

Thus, we obtain a spin temperature of $T_S = 146.8 \pm 10.7$ K and hydrogen density $n = 0.89 \pm 0.14$. We list the values in Table 1 in comparison with the other estimations using the saturated temperatures in the VDR. A simple mean of the listed three values with an equal weight yields $T_S = 145.8 \pm 1.2$ K, and we adopt this temperature for the analyses of Γ and τ.

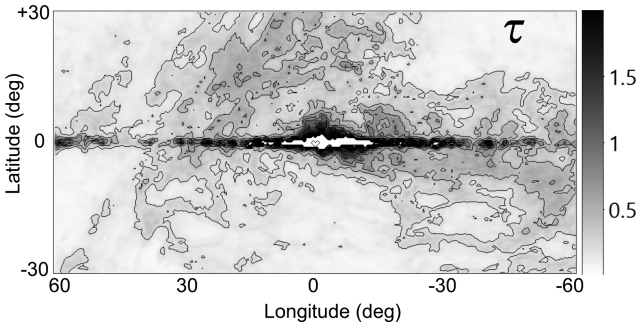

Figure 7. Optical depth τ. Contours start from 0.2 at intervals of 0.2.

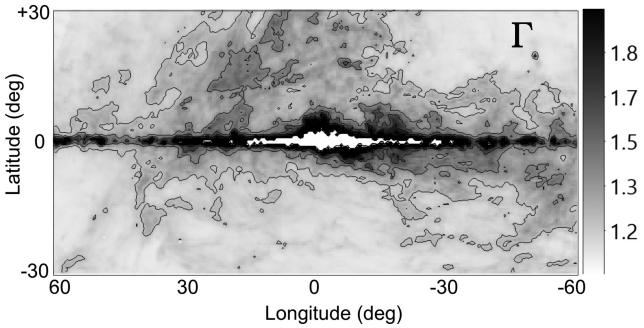

Figure 8. Grey-scale map of the correction factor Γ. Contours start from 1.2 at intervals of 0.2.

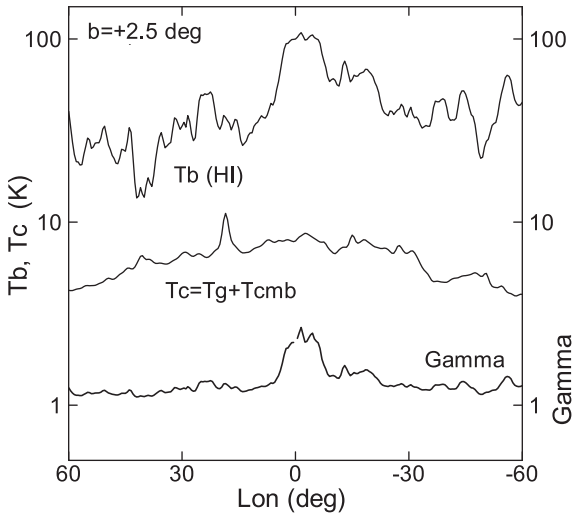

Figure 9. H I T_B at $V_{LSR} = 0$ km s^{-1}, T_C at 1420 MHz, and the correction factor Γ, plotted against l at $b = +2.^\circ5$.

5 OFF-PLANE ANALYSIS FOR LOCAL H I

5.1 Γ, τ and corrected local H I map

Using the observed H I and continuum brightness temperatures, we calculated the distribution of the optical depth τ and the correction factor Γ on the sky, as shown in Figs 7 and 8, respectively.

Fig. 9 shows the variation of Γ against longitude at fixed latitude $b = 2.^\circ5$ compared to those for the brightness temperatures of H I and continuum emissions. Fig. 10 shows the Γ distribution at different latitudes.

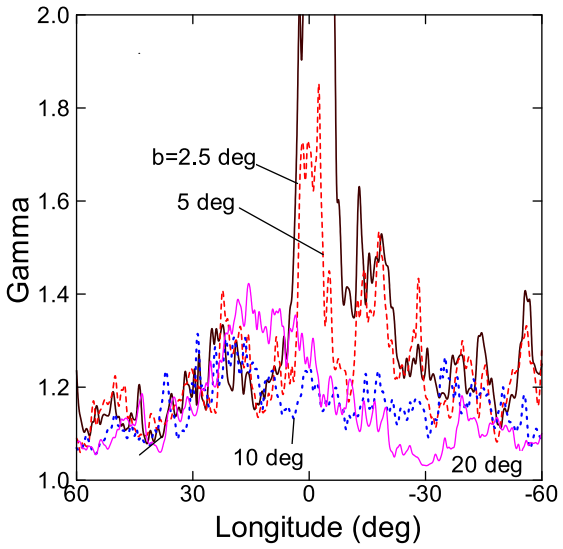

Figure 10. Γ versus l at different b.

Table 2. Mean and standard deviation of the correction factor Γ and optical depth τ.

Region, l deg $\pm\Delta l/b$ deg range	Γ	τ
Off-Galactic plane		
$0.0 \pm 60/b = -30 \sim -5$	1.22 ± 0.12	0.24 ± 0.15
$0.0 \pm 60/b = +5 \sim +30$	1.17 ± 0.08	0.18 ± 0.11
Galactic plane minima, inter-VDR		
40.0 ± 10.0	1.36 ± 0.14	0.43 ± 0.18
130.0 ± 10.0	1.26 ± 0.06	0.44 ± 0.10
230.0 ± 10.0	1.14 ± 0.06	0.20 ± 0.10
310.0 ± 10.0	1.47 ± 0.17	0.64 ± 0.25
Average[a] local	1.22 ± 0.03	0.30 ± 0.05
VDR, solar circle (arm)		
75.0 ± 5.0	1.84 ± 0.23	1.32 ± 0.31
280.0 ± 5.0	2.19 ± 0.67	1.68 ± 0.81
VDR, anti-Centre		
180.0 ± 5.0	1.77 ± 0.13	1.23 ± 0.18
Average arm + anti-Centre	1.80 ± 0.11	1.27 ± 0.15
VDR, GC		
0.0 ± 5.0	3.63 ± 0.82	2.66 ± 0.86
0.0 ± 10.0	3.36 ± 0.86	2.53 ± 0.86

[a]Average of the individual regions in the distance category using their standard deviations as the weights.

The Γ value is observed to be around $\Gamma \sim 1.2$ at $b > \sim 2.^\circ5$ and $|l| > \sim 30^\circ$. It becomes larger near the Galactic plane at $b < 2.^\circ5$. In some regions towards known H I clouds, Γ attains higher values even at higher latitudes.

In Table 2, we list typical values averaged in the off-plane regions enclosed by the box shown in Fig. 1. An averaged value of $\Gamma \sim 1.2$ was obtained for the local H I gas. The slightly larger value in the northern half of the region would be due to the contamination of the Aquila Rift.

Using the maps thus obtained for τ and Γ combined with the H I brightness map at V_{LSR}, we finally calculated the volume density of H I gas using equation (17). The result of the volume density distribution on the sky is shown in Fig. 11.

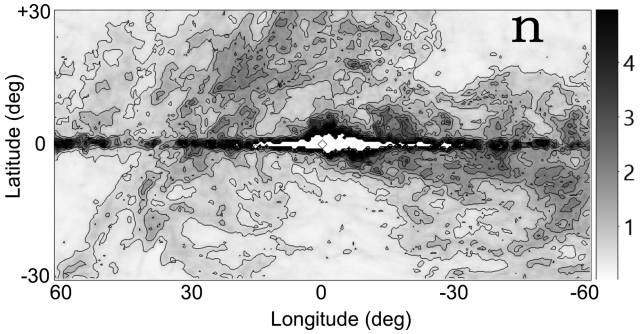

Figure 11. Distribution of the volume density of local H I gas, n. Contour interval is 0.5 H cm^{-3}.

Using the map, avoiding the near-Galactic plane region, we determined the local H I density to be $n = 0.86 \pm 0.52$ H cm^{-3} in the northern area at $b \geq 5^\circ$, and $n = 0.69 \pm 0.46$ H cm^{-3} in the south at $b \leq 5^\circ$. These values are consistent with the value, $n = 0.89 \pm 0.14$ H cm^3, obtained using the χ^2 fitting of T_B to the region around the VDR near the Galactic plane, as shown in Table 1.

6 GALACTIC-PLANE ANALYSIS FOR GLOBAL H I

6.1 Γ and τ in the Galactic plane

In the previous analysis of local H I gas, we avoided the saturated regions in the VDR and the Galactic plane. However, equation (13) applies to any regions for measured T_B and T_C. In fact, Fig. 10 shows higher Γ towards the Galactic plane.

In order to analyse Γ and τ in the Galactic plane, we replace the radio continuum brightness given by equation (1) with brightness for a mixed case in which thermal and synchrotron emissions coexist using equation (2). In fact, thermal radio sources such as H II regions are tightly concentrated to a thin galactic disc of full thickness ∼90 pc (Hou & Han 2014; Sofue & Nakanishi 2017b).

Note, however, that we put the galactic continuum emission to zero in the longitude range from $l = 70^\circ$ to 200°, where no Rhodes continuum data are available. According to equation (13), this approximation may cause a slight systematic underestimation of Γ of the order of $\sim 10^{-2}$, but the amount is within the measurement error. This is because T_B in this longitude range is considered to be less than a few K and is much lower than T_S.

We show the variation of Γ and τ thus calculated along the Galactic plane in Fig. 12, where the values are averaged in longitude bins of 5° width. The bars are standard deviations in the bins. Grey dots show raw values before averaging.

In Table 2, we list the measured values of Γ and τ along the Galactic plane ($b = 0^\circ$). The listed values are mean Γ and τ in representative directions in the Galactic plane ($b = 0^\circ$) at l within $\pm\Delta l$ from the indicated longitudes. The mean was obtained by taking the Gaussian-running average in each longitudinal bin of half-width of 5°.

6.2 Local value of Γ in the inter-VDR directions

Values close to unity with Γ ∼ 1.2 were obtained in the off-arm directions, where the line-of-sight depth is less than a few hundred pc corresponding to the velocity range around $V_{LSR} = 0$ km s^{-1}. Therefore, the local H I gas is optically thin even in the Galactic plane, and it is consistent with the off-plane local values as listed in Table 2. The values obtained in individual regions, including those for the off-Galactic plane regions, are further averaged using their standard deviations as weights, and listed as the mean of the local Γ and τ values in the row below the category in Table 2. It is interesting to note that the values are close to that obtained in the Perseus arm (Lee et al. 2015).

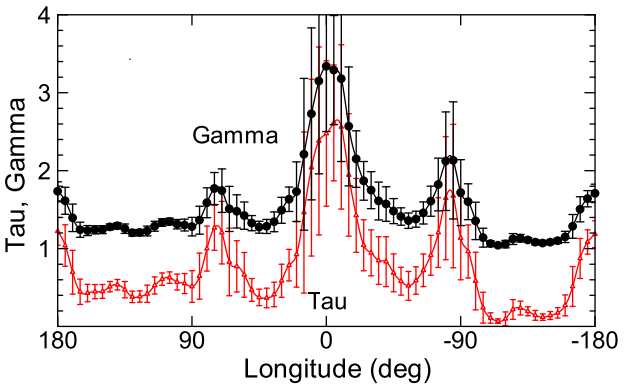

Figure 12. Γ (black circles) and τ (triangles) in the Galactic plane averaged in longitude bins of ±5° width. Bars indicate standard deviations.

6.3 Modest Γ in the local arm direction

Values of about Γ ∼ 2 were obtained in the directions of the local arms as well as in the anti-Centre direction. The line-of-sight depths in these directions are several kpc, and the H I mass in the disc in the vicinity of the Sun may be doubled. This value can be compared with the values observed for H I gas in circum-molecular cloud regions by Fukui et al. (2014), who argued for a significant amount of cold H I gas hidden behind optically thick H I as well as dark clouds.

6.4 High Γ correction in the GC direction

A high correction factor of Γ ∼ 3.6 ± 0.8 was obtained close to the GC at $|l| \leq 5^\circ$, and 3.4 ± 0.9 at $|l| \leq 10^\circ$. This high Γ means that the Galactic disc between the Sun and the GC is more abundant in H I gas with density a factor of ∼3–4 times higher than those so far derived for the optically thin assumption. In fact, it has long been thought that H I is deficient in the inner Galaxy at $R \sim 8$ kpc, where molecular gas is dominant over H I (Nakanishi & Sofue 2003, 2006, 2016), but this might not be the case when the finite optical thickness is taken into account.

If such high Γ correction is applied to the H I density map of the Galaxy (Nakanishi & Sofue 2003, 2006, 2016), we might need to reconsider the ISM composition in the Galaxy. It might increase the H I mass by several times in the inner Galaxy. It will affect the ISM physics such as the study of molecular fraction, and the H I to H_2 phase transition theory as well as the star formation efficiently via the Schmidt law (Sofue & Nakanishi 2016, 2017b). Because the dynamical mass distribution has been independently determined using the rotation curve, the fractional/abundance consideration of the stellar versus ISM components in the inner Galaxy may be revised by such an increase in the H I mass.

7 SUMMARY AND DISCUSSION

7.1 Summary

We derived a formula to calculate the ratio Γ of volume density of H I gas with finite optical thickness to that under the assumption of low opacity. The ratio can be used as a correction factor

to estimate the H I densities from currently derived values for the optically thin assumption. We presented a map of the Γ values on the sky and a corrected map of the local H I density n in the solar vicinity.

In order to apply the method, we determined the spin temperature T_S using the saturated brightness in the VDR towards the GC and a local arm, and we obtained $T_S \simeq 146.2 \pm 16.1$ K and 144.4 ± 6.8 K, respectively. We also applied the least χ^2 fitting to the T_B distribution in the Galactic plane at $|l| \leq 30^\circ$ around the VDR. We obtained the best-fitting set of T_S and n to be $T_S = 146.8 \pm 10.7$ K and $n = 0.89 \pm 0.14$. Considering these values, we adopted $T_S = 146$ K in the analysis for Γ.

The local value of the correction factor was obtained to be $\Gamma \sim 1.2$ in the off-Galactic plane region, and $\Gamma \sim 1.3$ in the inter VDR (off-solar circle) directions in the Galactic plane. Thus, the local H I density (e.g. within 100–200 pc around the Sun) will be larger by a factor of $\sim$1.2 than the currently estimated density.

A modest value of $\Gamma \sim 2$ was obtained in the VDR towards local arm (solar circle) and anti-Centre directions. These indicate higher H I mass in the spiral arms and Galactic disc at $R \sim 8$ kpc by a factor of $\sim$2 than the current density estimations.

A value as high as $\Gamma \sim 3.6 \pm 0.8$ was obtained in the VDR towards the GC at $|l| \leq 5^\circ$. This means that H I density, and therefore the mass, in the inner Galaxy is higher by a factor of $\sim$3–4 than the currently estimated density and mass under the assumption that the H I line is optically thin.

7.2 Limitation of the method

The recently developed method to determine the H I spin temperature was applied to the saturated H I brightness region at $V_{LSR} = 0$ km s^{-1} in the VDR as shown in Fig. 2. Although we have shown the result for $V_{LSR} = 0$ km s^{-1} as a typical example, this method can also be applied to other velocities, if the H I brightness is saturated in the considered region.

Using the spin temperature, the brightness temperature is related to the volume density through equations (10) and (12), because the term dv/dx is a known quantity from the rotation curve. Thus, the column density N, which is an integration of spectral distribution of T_B in a finite velocity range, is not used in the present analysis. In this sense, the present method is not a general method to measure typical H I clouds, but is a specific method for the VDR in the Galactic disc with known kinematics, as shown in Fig. 2.

7.3 WNM shadowed by CNM

We have so far assumed that the H I gas is composed of a single component either of CNM or WNM, and that the spin temperature is constant in each component. However, the real ISM would be a mixture of both components (Field et al. 1969).

If the H I column is low and the CNM is optically thin, both the WNM and CNM emissions are observed simultaneously. This can in fact happen in inter-VDR directions, where the traditional use of equation (11) is valid regardless of the spin temperature, giving a reasonable estimation of the H I column density, because the equation does not include the spin temperature.

If the column density is so large that the CNM is optically thick, then H I line emission from the WNM is significantly absorbed, and the observed brightness temperature becomes saturated around the spin temperature of the CNM. In this case, the emission from the WNM is shadowed by the CNM.

Thus, it is difficult to detect the WNM on the same line of sight, as it is shadowed by the CNM. However, because the CNM and WNM are in thermal pressure equilibrium (Field et al. 1969), the density of the WNM is smaller than that of the CNM by a factor of $T_S(\mathrm{CNM})/T_S(\mathrm{WNM}) \sim 146\,\mathrm{K}/(2000 - 10^4)\,\mathrm{K} \sim 0.07$–$0.01$. The mass of the WNM on the same sight line would therefore be smaller than the CNM by a factor of 10–100. Hence, the correction for the CNM density and mass is a second-order problem, and does not affect the H I mass estimation significantly.

7.4 Uncertainty of T_S and propagation into Γ

We have assumed a constant spin temperature of $T_S = 146$ K according to the determination in Section 4. Hre, we note that the true spin temperature includes uncertainties arising from the following:

(i) the mixture effect of the CNM and WNM, which have quite different spin temperatures, while the effect was shown to be somehow suppressed by shadowing by the CNM, as above;
(ii) the variation due to intrinsic dispersion in inhomogeneous ISM composed of diffuse and dense cloud H I, as well as colder molecular clouds;
(iii) the larger-scale variation in the Galactic disc as a function of the galactocentric distance.

Although the temperature derived here already includes all these during the determination as an average, there might be some systematic effects, adding further uncertainty. We consider how such uncertainty propagates by giving artificial errors as $\delta T_S = 5$, 10 and 15 K.

Besides T_S, the continuum background brightness T_C estimated from the 2.3-GHz survey may include some systematic error such as that due to an incorrect spectral index and/or ratio of thermal to non-thermal emissions during the conversion from 2.3- to 1.4-GHz brightness. This effect would be of the order of a few K in the strongest region in the inner Galaxy, and would not be crucial in the present study within the estimation errors. For a more accurate analysis, this problem can be solved by using real 1.4-GHz continuum data at comparable resolutions; however, that is beyond the scope of this paper.

We now consider the propagation of δT_S into Γ, assuming that $T_C = 0$ K. When the gas is optically thin, T_S does not appear in the conversion relation from H I intensity to density, and hence δT_S does not affect Γ. If the gas is optically grey or thick, then δT_S included in the non-linear term propagates to the error in the correction factor, $\delta\Gamma$. For $T_C \ll T_S$, the propagation is approximated by

$$\frac{\delta\Gamma}{\Gamma} \simeq \frac{\delta T_S}{T_S}\left[\frac{1}{\Gamma(1 - T_B/T_S)} - 1\right]. \tag{24}$$

Fig. 13 shows the variation of $\delta\Gamma$ as a function of T_B/T_S for $\delta T_S = 5$, 10 and 15 K. It is readily seen that $\delta\Gamma$ is small at $T_B < \sim 0.8 T_S$, or at $T_B < \sim 120$ K for $T_S = 146$ K. Although $\delta\Gamma$ increases steeply beyond, it is still sufficiently small when δT_S is less than $\sim$10 K.

If δT_S is larger (e.g. $> \sim 15$ K), then $\delta\Gamma$ becomes comparable or greater than Γ at $T_B > \sim 140$ K. This will be crucial only in the VDR towards the GC, where we found high Γ and T_B. However, considering the procedure of determining T_S in Section 4, such a large uncertainty should not be present. Therefore, we can consider

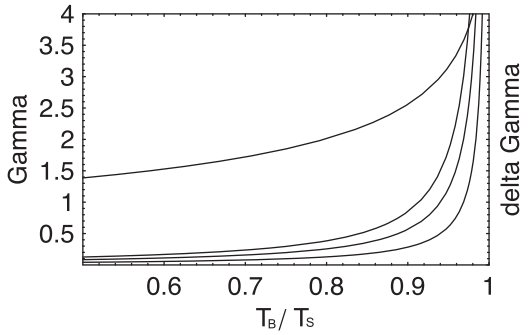

Figure 13. The error $\delta\Gamma$ in the correction factor propagating from the uncertainty δT_S of the spin temperature, plotted against T_B/T_S for three cases of $\delta T_S = 5$, 10 and 15 K (from bottom to top) and $T_S = 146$ K. The uppermost curve shows Γ.

that the present measurements may not be changed largely within the errors.

ACKNOWLEDGEMENTS

The author is indebted to Prof. P. M. Kalberla and the coauthors for the data base of the Leiden-Argentine-Bonn (LAB) All-Sky H I-Line Survey.

REFERENCES

Brown C., Dickey J. M., Dawson J. R., McClure-Griffiths N. M., 2014, ApJS, 211, 29
Chengalur J. N., Kanekar N., Roy N., 2013, MNRAS, 432, 3074
Dickey J. M., McClure-Griffiths N. M., Gaensler B. M., Green A. J., 2003, ApJ, 585, 801
Field G. B., Goldsmith D. W., Habing H. J., 1969, ApJ, 155, L149
Fukui Y. et al., 2014, ApJ, 796, 59
Fukui Y., Torii K., Onishi T., Yamamoto H., Okamoto R., Hayakawa T., Tachihara K., Sano H., 2015, ApJ, 798, 6
Goldsmith P. F., Li D., 2005, ApJ, 622, 938
Heiles C., Troland T. H., 2003a, ApJ, 586, 1067
Heiles C., Troland T. H., 2003b, ApJS, 145, 329
Hou L. G., Han J. L., 2014, A&A, 569, A125
Jonas J. L., de Jager G., Baart E. E., 1985, A&AS, 62, 105
Kalberla P. M. W., Burton W. B., Hartmann D., Arnal E. M., Bajaja E., Morras R., Pöppel W. G. L., 2005, A&A, 440, 775
Kuchar T. A., Bania T. M., 1990, ApJ, 352, 192
Large M. I., Mathewson D. S., Haslam C. G. T., 1961, MNRAS, 123, 123
Lee M.-Y., Stanimirović S., Murray C. E., Heiles C., Miller J., 2015, ApJ, 809, 56
Li D., Goldsmith P. F., 2003, ApJ, 585, 823
Liszt H. S., 1983, ApJ, 275, 163
Liszt H. S., 2001, A&A, 371, 698
Liszt H. S., Braun R., Greisen E. W., 1993, AJ, 106, 2349
Mebold U., Winnberg A., Kalberla P. M. W., Goss W. M., 1982, A&A, 115, 223
Miyamoto M., Nagai R., 1975, PASJ, 27, 533
Murray C. E. et al., 2015, ApJ, 804, 89
Nakanishi H., Sofue Y., 2003, PASJ, 55, 191
Nakanishi H., Sofue Y., 2006, PASJ, 58, 847
Nakanishi H., Sofue Y., 2016, PASJ, 68, 5
Roberts D. A., Goss W. M., Kalberla P. M. W., Herbstmeier U., Schwartz J. J., 1993, A&A, 274, 427
Roy N., Kanekar N., Braun R., Chengalur J. N., 2013a, MNRAS, 436, 2352
Roy N., Kanekar N., Chengalur J. N., 2013b, MNRAS, 436, 2366
Sofue Y., Nakanishi H., 2016, PASJ, 68, 63
Sofue Y., Nakanishi H., 2017a, MNRAS, 464, 783
Sofue Y., Nakanishi H., 2017b, PASJ, preprint (arXiv:1610.05396)
Sofue Y., Reich W., 1979, A&AS, 38, 251
Stark R., Dickey J. M., Burton W. B., Wennmacher A., 1994, A&A, 281, 199
Wolfire M. G., Hollenbach D., McKee C. F., Tielens A. G. G. M., Bakes E. L. O., 1995, ApJ, 443, 152

This paper has been typeset from a TEX/LATEX file prepared by the author.